Hearing Research 281 (2011) 74–83

Contents lists available at SciVerse ScienceDirect

Hearing Research

journal homepage: www.elsevier.com/locate/heares

Research paper

Restoration of 3D vestibular sensation in rhesus monkeys using a multichannel vestibular prosthesis

Chenkai Dai[a], Gene Y. Fridman[a], Natan S. Davidovics[a], Bryce Chiang[b], Joong Ho Ahn[a], Charles C. Della Santina[a,b,*]

[a] Department of Otolaryngology – Head & Neck Surgery, Johns Hopkins University School of Medicine, Baltimore, MD 21205, USA
[b] Department of Biomedical Engineering, Johns Hopkins University School of Medicine, 720 Rutland Ave., Ross Bldg Rm 830, Baltimore, MD 21205, USA

ARTICLE INFO

Article history:
Received 28 May 2011
Received in revised form
19 August 2011
Accepted 19 August 2011
Available online 26 August 2011

ABSTRACT

Profound bilateral loss of vestibular hair cell function can cause chronically disabling loss of balance and inability to maintain stable vision during head and body movements. We have previously shown that chinchillas rendered bilaterally vestibular-deficient via intratympanic administration of the ototoxic antibiotic gentamicin regain a more nearly normal 3-dimensional vestibulo-ocular reflex (3D VOR) when head motion information sensed by a head-mounted multichannel vestibular prosthesis (MVP) is encoded via rate-modulated pulsatile stimulation of vestibular nerve branches. Despite significant improvement versus the unaided condition, animals still exhibited some 3D VOR misalignment (i.e., the 3D axis of eye movement responses did not precisely align with the axis of head rotation), presumably due to current spread between a given ampullary nerve's stimulating electrode(s) and afferent fibers in non-targeted branches of the vestibular nerve. Assuming that effects of current spread depend on relative orientation and separation between nerve branches, anatomic differences between chinchilla and human labyrinths may limit the extent to which results in chinchillas accurately predict MVP performance in humans.

In this report, we describe the MVP-evoked 3D VOR measured in alert rhesus monkeys, which have labyrinths that are larger than chinchillas and temporal bone anatomy more similar to humans. Electrodes were implanted in five monkeys treated with intratympanic gentamicin to bilaterally ablate vestibular hair cell mechanosensitivity. Eye movements mediated by the 3D VOR were recorded during passive sinusoidal (0.2–5 Hz, peak 50°/s) and acceleration-step (1000°/s^2 to 150°/s) whole-body rotations in darkness about each semicircular canal axis. During constant 100 pulse/s stimulation (i.e., MVP powered ON but set to stimulate each ampullary nerve at a constant mean baseline rate not modulated by head motion), 3D VOR responses to head rotation exhibited profoundly low gain [(mean eye velocity amplitude)/(mean head velocity amplitude) < 0.1] and large misalignment between ideal and actual eye movements. In contrast, motion-modulated sinusoidal MVP stimuli elicited a 3D VOR with gain 0.4–0.7 and axis misalignment of 21–38°, and responses to high-acceleration transient head rotations exhibited gain and asymmetry closer to those of unilaterally gentamicin-treated animals (i.e., with one intact labyrinth) than to bilaterally gentamicin-treated animals without MVP stimulation. In comparison to responses observed under similar conditions in chinchillas, acute responses to MVP stimulation in rhesus macaque monkeys were slightly better aligned to the desired rotation axis. Responses during combined rotation and prosthetic stimulation were greater than when either stimulus was presented alone, suggesting that the central nervous system uses MVP input in the context of multisensory integration. Considering the similarity in temporal bone anatomy and VOR performance between rhesus monkeys and humans, these observations suggest that an MVP will likely restore a useful level of vestibular sensation and gaze stabilization in humans.

1. Introduction

In normal individuals, the two labyrinths modulate activity on afferent fibers within each branch of the vestibular nerve so as to provide the central nervous system with information regarding

* Corresponding author. Vestibular NeuroEngineering Laboratory, Johns Hopkins University School of Medicine, 720 Rutland Ave., Ross Bldg Rm 830, Baltimore, MD 21205, USA. Tel.: +1 410 502 7909; fax: +1 410 614 2439.
E-mail address: charley.dellasantina@jhu.edu (C.C. Della Santina).

0378-5955/$ – see front matter © 2011 Elsevier B.V. All rights reserved.
doi:10.1016/j.heares.2011.08.008

3-dimensional (3D) rotational head motion and linear acceleration due to gravity and translational motion. Vestibular sensory input drives compensatory reflexes that stabilize gaze and posture, maximizing clarity of vision during head movement, minimizing the risk of falling, and helping to maintain normal perception of body position and trajectory (Carey and Della Santina, 2005). Bilateral loss of vestibular sensation can occur as the result of ototoxic drug exposure, ischemia, infection, genetic abnormality, or trauma to the inner ears. Without a normal 3D vestibulo-ocular reflex (VOR) to keep images still on the retina, visual acuity falls dramatically during head rotations typical of walking, driving and other activities of daily life. In addition to this visual blur during head movement, bilaterally vestibular-deficient (BVD) individuals also suffer chronic disequilibrium and postural instability (Grunbauer et al., 1998; Minor, 1998; Gillespie and Minor, 1999).

There is no adequate treatment for individuals chronically disabled by profound bilateral vestibular deficiency (BVD) despite vestibular rehabilitation exercises intended to improve deficient vestibular reflexes via central adaptation. The lives of these BVD individuals could be significantly improved by an implantable neuroelectronic prosthesis that mimics the normal vestibular labyrinth by measuring head rotation, decomposing it into orthogonal components about the axes of the semicircular canals (SCCs), and selectively encoding it via electrical stimuli that recreate an appropriate pattern of activity in afferent nerve fibers of the corresponding ampullary branches of the vestibular nerve.

The Johns Hopkins Multichannel Vestibular Prosthesis (MVP) developed in our laboratory (Della Santina et al., 2005, 2007) senses angular velocity about three orthogonal axes and asynchronously stimulates each of the three ampullary nerves of an implanted labyrinth. This device achieves partial restoration of VOR responses for head rotation about any axis in BVD chinchillas (Della Santina et al., 2005, 2007; Fridman et al., 2010; Davidovics et al., 2011; Dai et al., 2011). Noting the differences in temporal bone anatomy and size between chinchillas and the chronically disabled human subjects for whom the MVP was developed, we sought to extend that approach to rhesus monkeys, which have temporal bone anatomy very similar to that of humans. Because the separation between different vestibular nerve branches in the rhesus labyrinth is about $\sim$1.5–1.7$\times$ greater than in chinchillas (Della Santina, unpublished observations), we hypothesized that rhesus monkeys would exhibit findings at least as close to normal (in terms of 3D VOR alignment and asymmetry) as those we have observed in chinchillas. We also sought to examine whether prosthetic input delivered by the MVP leads to different responses depending on whether it is congruent with other sensory input (i.e., delivered during actual whole-body rotation) or incongruent with it (e.g., delivered to an animal that is actually stationary).

2. Methods

2.1. Animal subjects

Five rhesus monkeys (5–7 kg, 4 female and 1 male) were used for all experiments, which were performed in accordance with a protocol approved by the Johns Hopkins Animal Care and Use Committee, which is accredited by the Association for the Assessment and Accreditation of Laboratory Animal Care (AAALAC) International and consistent with European Community Directive 86/609/EEC.

2.2. Experimental design overview

Prior to any manipulation of the labyrinths, 3D VOR responses of normal monkeys were measured in response to whole-body, passive sinusoidal and impulse rotations delivered in darkness about each of the mean SCC axes. Responses were also measured during brief steps of passive, whole-body rotational acceleration in darkness except for a centering fixation target. An MVP electrode array was then implanted in the left labyrinth of each animal, and both labyrinths were treated with intratympanic gentamicin injections to ablate vestibular hair cell mechanosensitivity. Once severe/profound reduction in VOR eye movement responses to whole-body rotation without prosthetic stimulation was confirmed, animals were adapted in light to a baseline, constant stimulation rate of 94 pulse/s (pps) on each of 3 ampullary nerve stimulating electrodes until slow phase nystagmus with the head stationary (an effect of asymmetry in baseline vestibular nerve activity between the implanted and nonimplanted labyrinths) reduced to $<3^\circ$/s. Animals were then tested for 3D VOR responses about each mean SCC axis under three experimental conditions: (1) passive whole-body rotations in darkness with only constant-rate prosthetic stimulation (*mechanical-only* condition); (2) pulse-frequency-modulated prosthetic electrical stimulation with the monkey stationary (*prosthesis-only* condition); and (3) whole-body rotation during prosthetic stimulation rate-modulated for each ampullary nerve channel by the MVP sensor detecting head motion about the corresponding axis (*combined* condition).

2.3. Surgical procedures

Our methods used for surgical implantation of a head-fixation mechanism and scleral coils for magnetic search coil recording of 3D eye movements in primates have been described previously (Minor et al., 1999; Lasker et al., 2000; Chiang et al., 2011). With the animal under general inhalational anesthesia (2–5% isoflurane), a light poly-ether-ether-ketone head cap was affixed to the skull under sterile conditions using titanium bone screws and polymethyl methacrylate. Two search coils were fashioned from polytetrafluoroethylene-coated steel wire (Cooner Wire, Chatsworth, CA) and sutured to the sclera of one globe, with one around the iris and the other approximately orthogonal to the first. Wires were tightly twisted to reduce inductive artifacts and then run to connectors within the head cap. Animals were maintained under general anesthesia for surgery and treated with analgesics and antibiotics for 72 h perioperatively.

After characterization of a normal animal's VOR responses, an electrode array was implanted into the left labyrinth via a transmastoid approach analogous to that used for cochlear implantation (Dai et al., 2010; Chiang et al., 2011). Under sterile conditions, a mastoidectomy was performed. The junction of the ampullae of the superior and horizontal SCCs was identified, and two small holes were made there, keeping a thin strut of bone intact between the two to serve as a stop when inserting the forked electrode array. An opening was also made in the thin segment of the posterior SCC near its junction with the ampulla, into which the single-tine electrode array was inserted. Pieces of fascia were tucked around each array, and a small amount of dental cement (Protemp ESPE, 3M Corp) was used to stabilize the electrode leads, which were run under periosteum to the head cap. Fig. 1 shows a 3D surface (Fig. 1A) and oblique slice (Fig. 1B) reconstructed from a high-resolution computed tomography (CT) scan of an implanted rhesus monkey.

Intratympanic gentamicin was administered using a regimen similar to that used in humans (Carey et al., 2002), except that the animal was maintained under general inhalational anesthesia (2–5% isoflurane) for 30 min with the treated ear up to help ensure adequate diffusion of drug across the round window and into the inner ear. For each treatment, $\sim$0.5 mL of 26.7 mg/mL buffered gentamicin solution injected through the ear drum into the middle

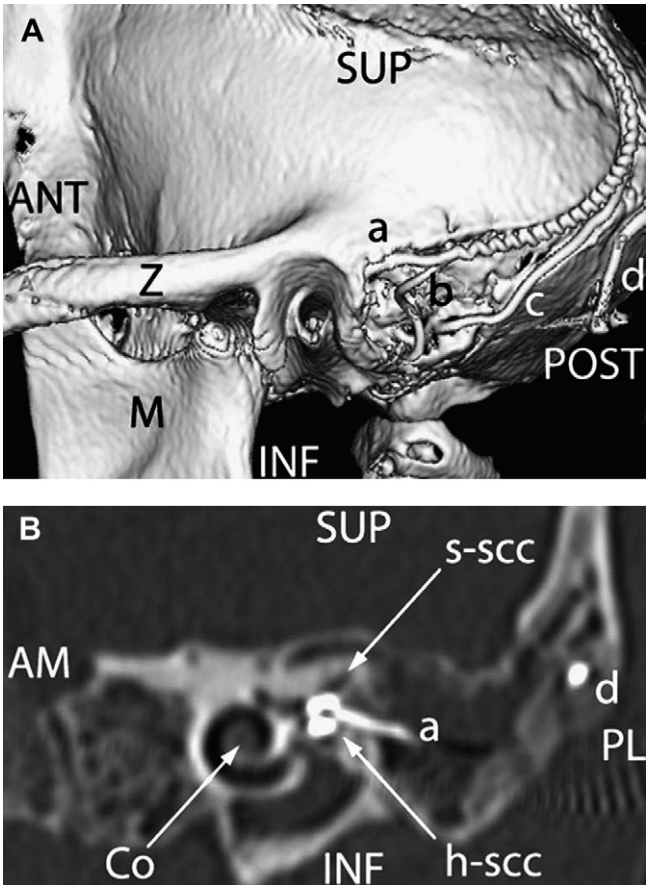

Fig. 1. Electrode array placement. (A) Posterolateral view of 3D CT surface reconstruction showing electrode array leads implanted in the left labyrinth of a rhesus monkey via the mastoid cavity. a: lead to anterior and horizontal ampullae; b: lead to posterior ampulla; c: common crus reference electrode; d: neck reference electrode; M: mandibular ramus; Z: zygomatic arch; ANT, POST, SUP, INF: anterior, posterior, superior, inferior. (B) Oblique CT cut through the plane of the basal turn of the cochlea [Co], showing bifurcated electrode array [a] entering the ampullae of the superior [s-scc] and horizontal [h-scc] semicircular canals. Part of the neck reference electrode [d] is also visible, but the posterior SCC electrode array is not included in this section. AM, PL: anteriomedial, posterolateral. (Reproduced with permission from Dai et al., 2010).

ear. Delivered via this route, gentamicin accumulates in hair cells and ultimately ablates labyrinthine mechanosensitivity by destroying Type I hair cells and by denuding Type II hair cells of their stereocilia (Hirvonen et al., 2005; Lyford-Pike et al., 2007). Treatments were repeated each three weeks until VOR responses to head rotation toward the treated ear reduced to <10% of normal gain, which required two or three injections per ear in each case. About half of human patients treated with intratympanic gentamicin for Ménière's disease require more than one injection to achieve the desired drop in labyrinthine function (Nguyen et al., 2009).

2.4. Stimulation paradigms

2.4.1. Rotational stimulation

To characterize the 3D VOR driven by labyrinthine mechanosensitivity alone (*mechanical-only* condition), we measured VOR eye movement responses during passive sinusoidal (0.05–5 Hz, peak 50°/s) and acceleration-step (1000°/s^2 to 150°/s peak velocity) whole-body rotations delivered by a servo-controlled Earth-vertical axis rotator. Sinusoidal rotations were delivered in complete darkness. Although the monkey's body was unrestrained within its enclosure in the experimental apparatus, the head cap was rigidly coupled to a Fick gimbal holding the enclosure, allowing us to reorient the monkey as needed to bring each SCC axis in line with the Earth-vertical axis of the motorized rotator.

2.4.2. Prosthetic stimulation

We used a head-mounted Johns Hopkins MVP2 multichannel vestibular prosthesis (Chiang et al., 2011) with electrodes implanted in the left labyrinth. MVP circuitry was mounted within the head cap so as to align all three of its gyroscopes with the corresponding mean SCC planes. The head cap also contained three 3.7 V lithium ion batteries connected in parallel so that they could be replaced without interrupting power delivery to the MVP.

The MVP was programmed to deliver symmetric biphasic, charge balanced, 200 μs/phase and 100–200 μA/phase pulse trains via each of three ampullary electrodes with respect to a return electrode in the common crus of the left labyrinth. Each biphasic pulse comprised three fixed-duration intervals: a constant-current cathodic phase (during which the active electrode near the target nerve was cathodic and a reference electrode was anodic), a 25 μs zero-current interphase gap, and a charge-balancing constant-current anodic phase during which the direction of current flow was reversed. Instantaneous pulse rate was defined as the reciprocal of the time from onset of one cathodic phase to the onset of the next. Pulses were presented concurrently but asynchronously, with only one electrode pair active at any given moment.

We determined the stimulation current amplitude for each electrode by gradually increasing the current amplitude of 200 μs/phase symmetric constant-current biphasic pulse trains modulated between 0 and 400 pulse/s (pps) at 1 Hz while we measured 3D eye movements with the stationary animal sitting upright in darkness. For each electrode, we set the stimulus current at a level that evoked near-maximal eye movements aligned with the axis of that electrode's SCC without eliciting signs of facial nerve activation. This current was then kept constant for all subsequent tests.

Pulse rates were modulated to encode MVP rotational velocity sensor inputs using a scheme described in detail elsewhere (Della Santina et al., 2007; Chiang et al., 2011). In brief, the baseline stimulation rate on each channel was 94 pulse/s. The operating curve mapping head velocity to pulse rate was designed to emulate normal rhesus vestibular afferent rate data reported by Sadeghi et al. (2007), which can be approximated by a sigmoidal relationship with 42, 94 and 175 pulse/s corresponding to −100, 0 and 100°/s, respectively, where positive values indicate head rotations excitatory for the implanted labyrinth. This was approximated by setting the MVP's mapping parameters (see Chiang et al., 2011) to $f_{\text{baseline}} = 100$ pulse/s, $f_{\max} = 350$ pulse/s, and $C = 2$ in the following equation:

$$f = 0.5 f_{\max}\left[1 + \tan h\left(A + C\left(\frac{x_i}{2018} - 1\right)\right)\right]$$
$$A = \tan h^{-1}\left(2 \times \frac{f_{\text{base}}}{f_{\max}} - 1\right) \quad (1)$$

where f is the output pulse rate, $f_{\max}$ is the peak pulse rate, f_{base} is the baseline stimulation rate for zero head velocity, C determines the slope of the pulse rate versus head velocity curve about the baseline rate, and x_i is a 12-bit digitized head velocity ranging from 0 (corresponding to 500°/s head rotation toward the implanted labyrinth) to 4095 (500°/s away), with 2048 corresponding to zero head velocity (See Fig. 2). The MVP's linear accelerometer inputs were not used.

To measure eye movements due solely to residual natural mechanosensitivity in animals that had been implanted and treated with gentamicin, (*mechanical-only* condition), we measured VOR responses to the same motion stimuli described in Section

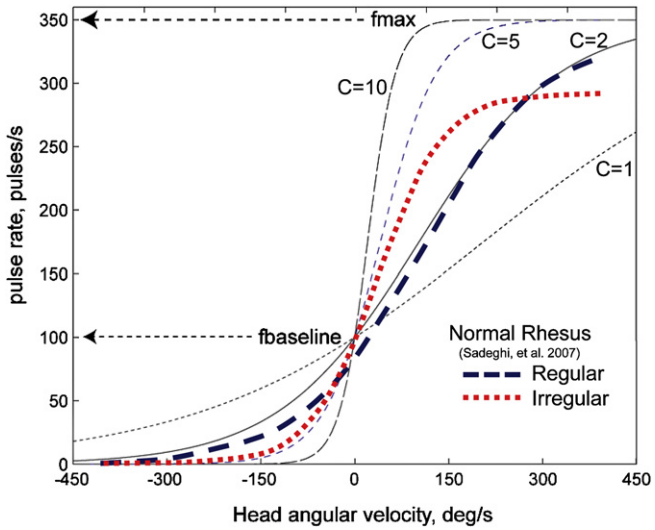

Fig. 2. Prosthesis pulse rate versus head velocity operating characteristic curves optionally employed by the MVP. Parameters shown correspond to those in Equation (1). The curve designated by $C = 2$ was used for all channels of the MVP in each monkey studied. The bold/dashed/blue and bold/dotted/red curves, respectively, depict mean firing rates of regular and irregular vestibular nerve primary afferents reported for normal rhesus monkeys by Sadeghi et al. (2007).

2.4.1 while the MVP was set to pulse on each of the three SCC channels with a constant mean rate of 94 pulse/s that did not modulate with head motion. To measure eye movements due solely to electrical stimulation (*prosthesis-only* condition), we measured VOR responses to prosthetic stimulation delivered with the head stationary and the animal seated upright in darkness. The MVP was directed to modulate pulse rates as if its sensors were encoding real sinusoidal 0.05–5 Hz, 50°/s peak rotations about each SCC axis, using the mapping functions previously defined. To measure VOR responses to combined electrical and rotational stimulation (*combined* condition), we then programmed the MVP to sense 3D head angular velocity and appropriately modulate the pulse rate on each channel of the MVP using the mapping functions previously defined, then applied the same passive sinusoidal and acceleration-step motion stimuli described in Section 2.4.1.

2.5. Eye movement measurement & analysis

The eye coil system we used to measure 3D angular eye position has been described in detail previously (Robinson, 1963; Migliaccio et al., 2004; Remmel, 1984). The monkey was seated in a plastic chair with its head restrained atraumatically by the skull cap. The chair was mounted atop the Earth-vertical axis rotator within a gimbal that allowed us to reorient the animal to align any SCC axis with that of the rotator. Counterclockwise motor rotation as viewed from above was considered a *positive* sense rotation in each case, and the animal was oriented as necessary to adhere to the right-hand-rule coordinate system convention used previously to describe 3D VOR data (Migliaccio et al., 2004). For example, a positive horizontal (yaw) rotation was delivered with the animal erect, and it excited the left horizontal SCC while inhibiting the right horizontal SCC. LARP axis rotations were delivered with the animal positioned supine after its head was first reoriented to turn the nose 45° toward the left ear; a positive LARP rotation excited the *right* posterior SCC and inhibited the left anterior SCC. RALP axis rotations were delivered with the animal positioned supine after its head was first reoriented to turn the nose 45° toward the right ear; a positive RALP rotation excited the *right* anterior SCC and inhibited the left posterior SCC. (A potentially confusing side effect of this standard convention is that excitation of the left labyrinth, as occurs during increases in MVP stimulation rates on that side, elicits VOR responses with horizontal, LARP and RALP components that are *negative*, positive and positive, respectively.)

Three pairs of field coils were rigidly attached to the superstructure and moved with the animal, generating three fields orthogonal to each other and aligned with the *X* (nasooccipital, +nasal), *Y* (interaural, +left), and *Z* (superoinferior, +superior) head coordinate axes. The *X*, *Y* and *Z* fields oscillated at 79.4, 52.6 and 40.0 kHz respectively. The three frequency signals induced across each scleral coil were demodulated to produce three voltages proportional to the angles between the coil and each magnetic field, then analyzed using 3D rotational kinematic methods detailed by Straumann et al. (1995). All signals transducing motion of the head or the eye were passed through eight-pole Butterworth anti-aliasing filters with a corner frequency of 100 Hz prior to sampling at 200 Hz. Coil misalignment was corrected using an algorithm that calculated the instantaneous rotation of the coil-pair with reference to its orientation when the eye was in a reference position (Tweed et al., 1990). Angular rotations were expressed as rotation vectors with roll, pitch, and yaw coordinates, and angular velocity vectors of eye with respect to head were calculated from the corresponding rotation vectors (Haslwanter, 1995; Migliaccio and Todd, 1999; Hepp, 1990). Angular position resolution of the coil system was 0.2° (tested over the angular range of ±25° combined yaw, pitch, and roll positions), and angular velocity noise was ~2.5°/s peak.

For responses to sinusoidal stimuli, each of the three eye movement components (horizontal, LARP, and RALP) were separately averaged for >10 cycles free of saccades and blinks. LARP and RALP axes were approximated as being 45° off the midline and in the mean plane of the horizontal SCCs. For each component of each response and for each stimulus trace, we used a single-frequency Fourier analysis to compute the magnitude of the single, symmetric best-fit sinusoid to the response, under the constraint that the response frequency was the same as the known stimulus frequency.

For responses to steps of acceleration, we computed the "acceleration gain" ratio (G_A) of eye to head velocity ratio averaged over the constant-head-acceleration segment of the record, prior to the onset of the first nystagmus quick phase. This method is described in detail elsewhere (Minor et al., 1999; Migliaccio et al., 2004, 2010). Only the main component of the 3D VOR was used to compute G_A. Data from 10 to 20 stimulus trials in each direction were averaged to obtain a representation of the response. For each trial, response latency was computed as the time difference between the zero-velocity-intercept times for the best-fit lines approximating the constant-acceleration segment of mean eye and head velocity traces. These times were measured using the iterative linear fit method described in Migliaccio et al. (2004).

To compare VOR gains, phases, G_A values and latencies across animals, frequencies, SCC axes and rotation half cycles, we used ANOVA followed when indicated by post hoc tests, with $p < 0.05$ considered significant.

3. Results

3.1. The 3D VOR of normal rhesus monkeys during passive whole-body rotations

3.1.1. Responses to sinusoidal rotations

Fig. 3A–C shows mean cycle-averaged head and eye angular velocities of a normal rhesus monkey (M067RhF) during 20 cycles of

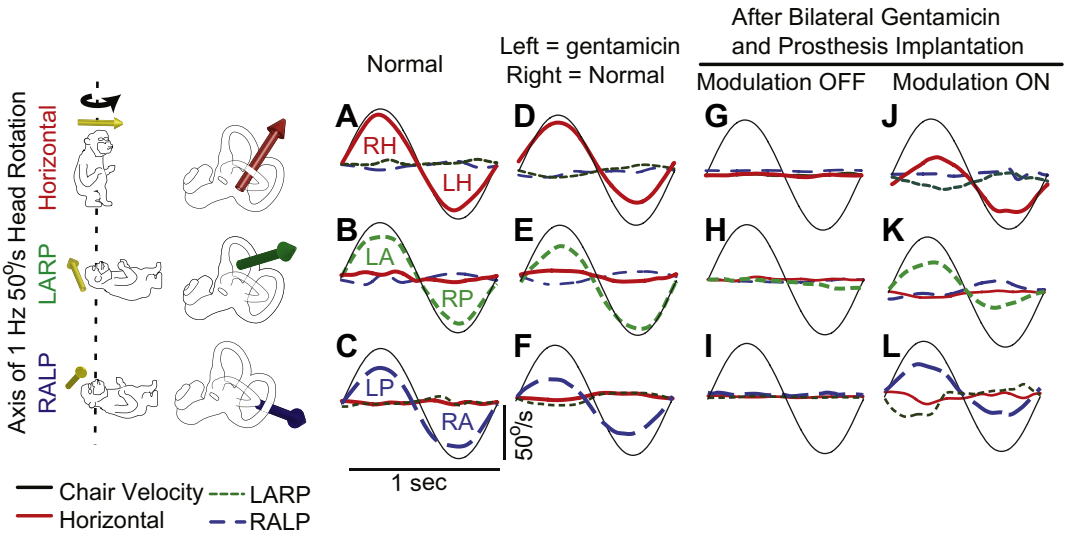

Fig. 3. Mean eye and head angular velocities of normal and vestibular-deficient rhesus monkeys during 2 Hz, 50°/s head rotations in darkness about the horizontal (top row), left-anterior/right-posterior (LARP, middle row) and right-anterior/left-posterior (RALP, bottom row) SCC axes. Monkeys were reoriented as needed to align the SCC axis of interest with the rotating motor's Earth-vertical axis. The curved arrow depicts the sense of a positive polarity head rotation for each axis. In data traces, head velocity is inverted to facilitate comparison, and eye velocities are displayed using the convention described it the text, for which excitation of the left horizontal (LH), left anterior (LA) and left posterior (LP) SCCs elicits *negative* horizontal, positive LARP and positive RALP half cycles of eye movement. A–C: Normal monkey prior to electrode implantation and gentamicin treatment. For comparison to the asymmetric responses of monkeys tested under other conditions, the SCC predominantly *excited* during each half-cycle is labeled. This pattern is the same for all data shown. D–F: After unilateral gentamicin treatment of the left labyrinth, leaving the right ear normal. Note asymmetry of responses, with VOR gain greater for half cycles during right labyrinth excitation. G–I: After bilateral intratympanic gentamicin and electrode implantation in left labyrinth, with MVP pulsing at baseline rate on all channels but not modulating with head rotation. J–L: With MVP modulating to encode head rotation. Standard deviation of each trace at each time point is $<10°/s$. $N \geq 20$ cycles for each trace. Blinks and nystagmus quick phases were removed from analysis prior to averaging.

1 Hz, 50°/s peak passive, sinusoidal whole-body rotations in darkness about the mean horizontal (top row), left-anterior/right-posterior (LARP, middle row) and right-anterior/left-posterior (RALP, bottom row) SCC axes. The mean gain for the main VOR component (i.e., about the axis of head rotation) was 0.95 ± 0.08, 0.81 ± 0.12 and 0.78 ± 0.07 (means $\pm$ SD, $N > 20$ cycles) for rotations about the horizontal, LARP and RALP axes, respectively. Components about other axes are small, indicating a well-aligned 3D VOR response.

Mean gain and phase characteristics for the main component of VOR responses to 0.05–5 Hz, 50°/s sinusoidal rotations in darkness

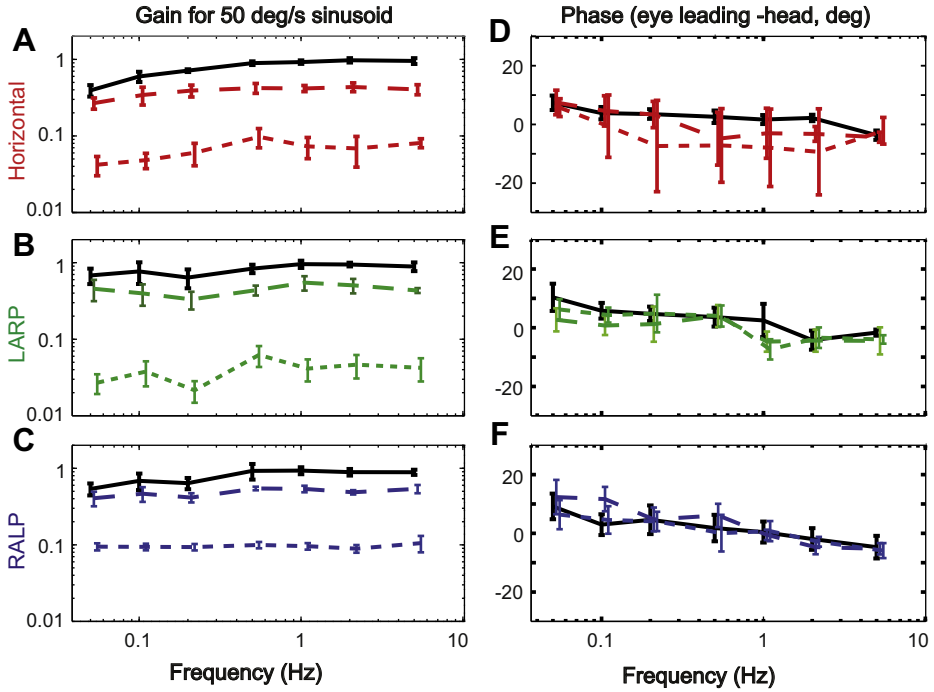

Fig. 4. Mean $\pm$ SD gain (A–C) and phase (D–F) of slow phase eye movements with respect to the ideal response ($-1 \times$ head velocity) for the main component of the 3D VOR response during sinusoidal horizontal (A,D), LARP (B,E) and RALP (C,F) for rhesus monkeys during 50°/s peak, 0.05–5 Hz, passive whole-body rotation in darkness. Solid lines: Normal monkeys ($N = 5$). Dashed lines: Monkeys rendered bilaterally vestibular-deficient via intratympanic gentamicin treatment, with constant-rate MVP stimulation ($N = 4$). Dotted lines: Those same monkeys while receiving motion-modulated stimulation via a head-mounted multichannel vestibular prosthesis. Across all frequencies tested, modulated MVP stimulation restores a more normal response.

about the horizontal, LARP, and RALP SCC axes for all 5 normal monkeys are displayed in the solid traces of Fig. 4. Consistent with previous reports describing the 1D rhesus VOR during yaw rotations (Fetter and Zee, 1988; Sadeghi et al., 2006) and the 3D rhesus VOR during roll, pitch and yaw head rotations (Angelaki and Hess, 1994), the 3D VOR of normal rhesus monkeys during whole-body sinusoidal rotations about the horizontal, LARP and RALP axes exhibits a high-pass response characteristic, with yaw gains at 0.05 Hz being about half those at the highest frequencies examined. Gains for frequencies ≥0.5 Hz are close to 1 for all three SCC axes tested. A slight positive phase lead is evident at the lowest frequency tested, but phase leads are otherwise close to zero.

3.1.2. Responses to acceleration-step rotations

Fig. 5(A–C) shows cycle-averaged head and eye angular velocities of the a normal rhesus monkey (M067RhF, the same as in Fig. 3A–C) during 20 stimulus repetitions of 1000°/s^2 passive whole-body rotational acceleration steps to 150°/s peak velocity in darkness about the mean horizontal, LARP and RALP axes. The mean G_A for the VOR component about the axis of head rotation is symmetric for either rotation sense about each axis and, for stimuli exciting the left labyrinth, is equal to 0.98 ± 0.04, 0.93 ± 0.05 and 0.99 ± 0.04 for rotations about the horizontal, LARP and RALP axes, respectively. Components about other axes are small, indicating a well-aligned 3D VOR. The mean response latency is also symmetric and is equal to 8.4 ± 1.4, 9.5 ± 3.4 and 9.3 ± 0.9 ms for rotations about the horizontal, LARP and RALP axes, respectively.

Mean G_A and response latencies pooled across all 5 normal monkeys for each SCC axis (with data pooled across rotation senses for a given SCC axis) are shown in Fig. 6. Consistent with previous reports describing the 1D rhesus VOR during yaw rotations (Sadeghi et al., 2006; Fetter and Zee, 1988) and the 3D rhesus VOR during roll, pitch and yaw head rotations (Angelaki and Hess, 1994), the 3D VOR of normal rhesus monkeys during whole-body step rotations about the horizontal, LARP and RALP axes generates a nearly compensatory VOR at short latency. Responses are slightly higher in gain (0.98 ± 0.08) and lower in latency (8.4 ± 1.4 ms) for horizontal rotation stimuli than for LARP (G_A 0.85 ± 0.08; latency 10.7 ± 1.4 ms) or RALP stimuli (G_A 0.85 ± 0.06; latency 9.3 ± 0.9 ms). A multi-way ANOVA revealed that G_A is significantly higher ($p < 0.05$; $F = 6.84$, $F_{crit} = 5.32$) and the latency is significantly shorter ($p \leq 0.03$) for horizontal VOR responses than for

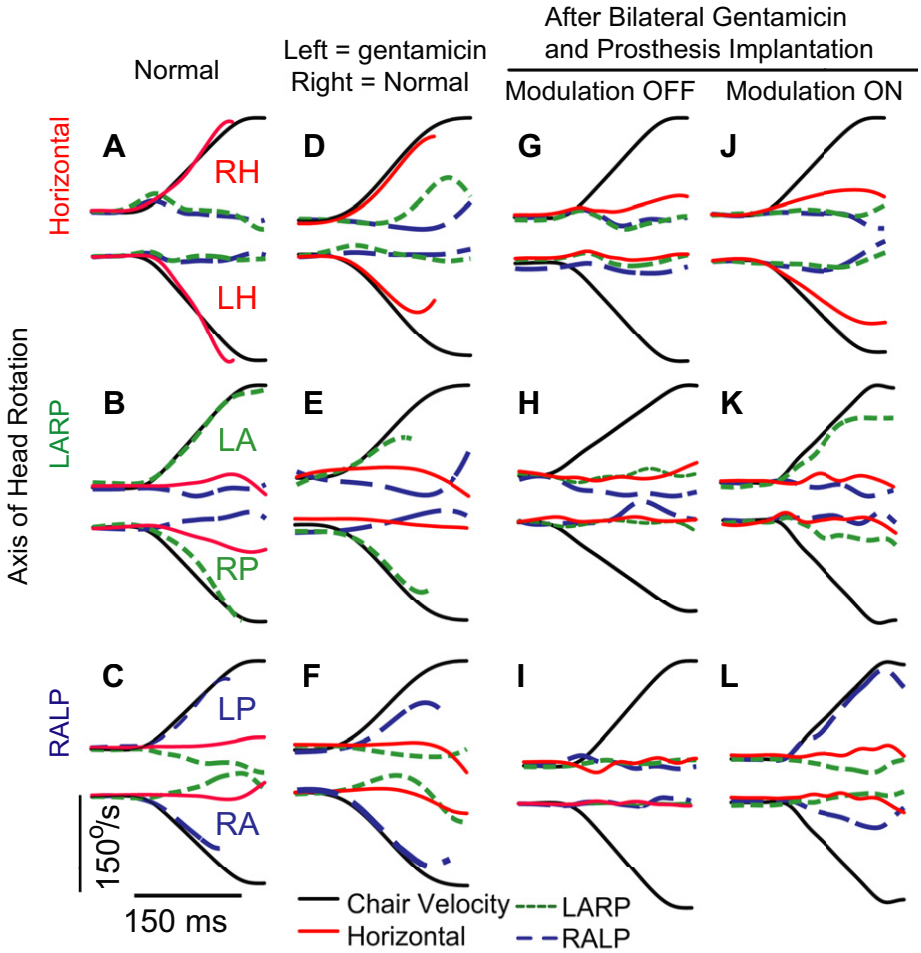

Fig. 5. (A–C): Mean ± SD eye and (inverted) head angular velocities of a normal rhesus monkey (M067RhF) during head impulse rotations (1000°/sec^2 to a peak head velocity of 150°/sec) in darkness, about the horizontal (A), left-anterior/right-posterior (LARP, B) and right-anterior/left-posterior (RALP, C) semicircular canal axes. Standard deviation of each trace at each time point is <10°/s. Data are truncated at the onset of the first nystagmus quick phase. Eye movement polarities conform to the convention described in the text and Fig. 3. The SCC being predominantly excited is designated for normal data here and consistent for all other panels. (D–F): Responses of the same monkey after left gentamicin treatment. Note the asymmetry of main component for each axis of rotation. (G–I): Same monkey after bilateral intratympanic gentamicin, plugging all SCCs, and electrode implantation in left labyrinth. Prosthesis pulsing at baseline stimulation rate of 100 pulse/s on each channel, but not modulating with head rotation. Responses are minimal, indicating failure of the VOR. (J–L): Same animal with motion-modulated MVP input. Although responses are still asymmetric, they are similar to those achieved by a single normal ear (compare panels D–F).

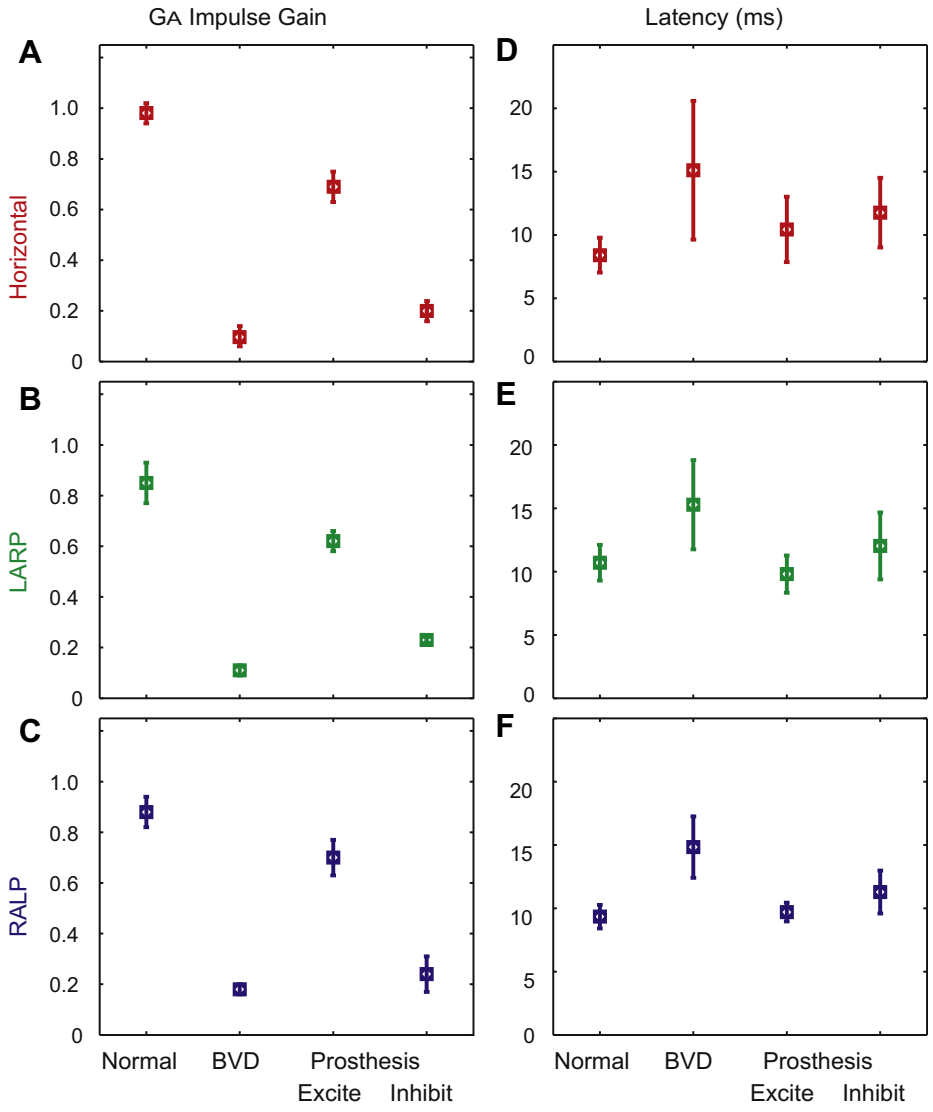

Fig. 6. Average acceleration gain (G_A) values (A–C) and latency (D–F) of the VOR measured during step of whole-body acceleration (1000°/s^2) to velocity plateau (150°/s) in darkness, about the horizontal (A,D), left-anterior/right-posterior (LARP – B,E) and right-anterior/left-posterior (RALP – C,F) SCC axes. Normal: Prior to electrode implantation and gentamicin treatment. BVD: After bilateral intratympanic gentamicin and electrode implantation in left labyrinth, with the MVP pulsing constantly but not at rates modulated by head motion. Prosthesis: With head motion modulated MVP input, during either head rotation toward (Excite) or away from (Inhibit) the implanted ear.

responses to stimuli about the other SCC axes, while responses about LARP and RALP axes were not significantly different from each other in major-component G_A or latency ($p = 0.11$; $F = 3.25$; $F_{crit} = 5.32$).

3.2. 3D VOR of rhesus monkeys after intratympanic gentamicin treatment

3.2.1. Responses to sinusoidal rotations

3.2.1.1. Unilateral gentamicin. Fig. 3D–F shows mean cycle-averaged head and eye angular velocities of monkey M067RhF after 3 rounds of intratympanic gentamicin treatment on the left side. (Prior to the third treatment, no drop in VOR performance was apparent.) The stimuli were the same as for Fig. 3A–C, i.e., 20 cycles of 1 Hz, 50°/s peak passive, sinusoidal whole-body rotations in darkness about the mean horizontal, LARP, and RALP axes. Responses are asymmetric, with larger half-cycle gain during excitation of the right labyrinth (0.94 ± 0.13, 0.95 ± 0.07 and 0.78 ± 0.14 for horizontal, LARP and RALP, respectively) than for during excitation of the left (0.52 ± 0.11, 0.63 ± 0.08 and 0.44 ± 0.10). This difference was significant (ANOVA: $p < 0.01$; $F = 13.25$; $F_{crit} = 7.71$). As for the normal condition data, components about other axes are small, indicating a well-aligned 3D VOR response.

3.2.1.2. Bilateral gentamicin and left MVP implantation, with non-modulated MVP stimulation. Fig. 3G–I shows mean cycle-averaged head and eye angular velocities of monkey M067RhF after left labyrinth MVP implantation and 3 rounds of intratympanic gentamicin treatment bilaterally. For these trials, the MVP was on and pulsing at approximately constant, baseline rates on each channel, but not modulating pulses rates to encode head velocity. The stimuli were the same as for Fig. 3A–F. The mean gain for the VOR component about the axis of head rotation was 0.08 ± 0.02, 0.04 ± 0.01 and 0.10 ± 0.01 for rotations about the horizontal, LARP and RALP axes, respectively. All components are small, indicating a grossly deficient 3D VOR response. Due to the weakness of responses, the degree of VOR misalignment is hard to quantify.

Mean gain and phase characteristics for the main component of VOR responses to 0.05–5 Hz, 50°/s sinusoidal rotations in darkness about the horizontal, LARP, and RALP SCC axes for 4 bilaterally vestibular-deficient (BVD) monkeys are displayed in the dotted traces of Fig. 4. The mean 3D VOR gain was less than about 10% of normal at every frequency, and phase was variable but close to zero.

3.2.2. Responses to acceleration-step rotations

3.2.2.1. Unilateral gentamicin. Fig. 5D–F shows mean cycle-averaged head and eye angular velocities of monkey M067RhF during acceleration steps after 3 rounds of intratympanic gentamicin treatment on the left side. The stimuli were the same as for Fig. 5A–C. Responses are asymmetric, with larger G_A during excitation of the right labyrinth (0.95 ± 0.07, 0.90 ± 0.10 and 0.92 ± 0.09 for horizontal, LARP and RALP, respectively) than for during excitation of the left (0.71 ± 0.12, 0.55 ± 0.13 and 0.58 ± 0.06). This difference was significant (ANOVA: $p < 0.01$; $F = 9.21$, $F_{crit} = 7.71$).

3.2.2.2. Bilateral gentamicin and left MVP implantation, with non-modulated MVP stimulation. Fig. 5G–I shows cycle-averaged head and eye angular velocities of monkey M067RhF after bilateral gentamicin treatment, left MVP implantation, and MVP activation with only a constant rate. The mean G_A for the VOR component about the axis of head rotation is symmetric for either rotation sense for each axis but small (0.10 ± 0.04, 0.11 ± 0.02 and 0.18 ± 0.02 for rotations about the horizontal, LARP and RALP axes, respectively), indicating a grossly deficient 3D VOR response with gains so low that the mean response latency and axis are difficult to quantify precisely.

Mean G_A and response latencies pooled both sides and across all 4 BVD monkeys for rotations about each SCC axis during non-modulated MVP stimulation are shown in Fig. 6. The 3D VOR of these monkeys is grossly deficient in all directions during acceleration steps. A multi-way ANOVA revealed that the gain is significantly lower ($p < 0.01$; $F = 10.20$, $F_{crit} = 5.32$) and the latency is significantly longer ($p < 0.01$; $F = 8.12$, $F_{crit} = 5.32$) than normal.

3.3. 3D VOR of BVD rhesus monkeys during motion-modulated MVP stimulation

3.3.1. Responses to sinusoidal rotations

Fig. 3J–L shows mean cycle-averaged head and eye angular velocities of monkey M067RhF after left labyrinth MVP implantation and 3 rounds of intratympanic gentamicin treatment bilaterally, with motion-modulated MVP input (i.e., the MVP set to perform according to its usual mode of operation). Motion stimuli were the same as for Fig. 3A–I. Some asymmetry in VOR responses is evident: half cycles of head rotation that excite the implanted labyrinth elicit greater responses than inhibitory half cycles, as was evident for the unilateral gentamicin/normal contralateral ear case (Fig. 3D–F) and as has been shown previously for unilaterally-implanted chinchillas (Della Santina et al., 2007; Fridman et al., 2010; Davidovics et al., 2011; Dai et al., 2011) and monkeys (Dai et al., 2010; Chiang et al., 2011) using the MVP. However, responses are sufficiently symmetric to fit the main component using a single sinusoid constrained to zero DC value. Using this parameterization, VOR gain was 0.58 ± 0.11, 0.44 ± 0.04 and 0.48 ± 0.05 for rotations about the horizontal, LARP and RALP axes, respectively. Other components were relatively small, consistent with a moderately well-aligned 3D VOR. Although neither the main component gain nor the 3D alignment are as close to perfect as observed when the animal was normal (Fig. 3A–C), VOR responses with the MVP are much larger than without modulated MVP stimulation (Fig. 3G–I) and symmetric to a degree similar to the unilateral gentamicin case of Fig. 3D–F (for which the one remaining normal ear's performance is a reasonable goal for an ear implanted with an MVP after bilateral gentamicin injury).

Mean gain and phase characteristics for sinusoidal rotations for 4 BVD monkeys with motion-modulated MVP stimulation are shown in Fig. 4 (dashed lines). For every frequency and stimulus rotation axis examined, the main component VOR gain was about half of normal and about 4 times larger than that observed without modulated MVP input. These differences were significant (ANOVA: $p < 0.01$). Phase responses during horizontal rotations were closer to normal than were responses without modulated MVP input, but there was no significant phase difference between stimulus conditions for LARP or RALP rotations ($p > 0.05$).

3.3.2. Responses to acceleration-step rotations

Fig. 3J–L shows cycle-averaged responses for monkey M067RhF during acceleration steps. These relatively high-acceleration stimuli unmask the excitation-inhibition asymmetry inherent in responses of an animal with only one labyrinth providing sensory input (Halmagyi and Curthoys, 1988; Fetter and Zee, 1988; Sadeghi et al., 2006). Mean G_A for the VOR component about the axis of head rotation was significantly larger, and response latency was significantly shorter, for head rotations that excite the implanted labyrinth than for inhibitory head rotations ($p < 0.01$; $F = 10.55$, $F_{crit} = 4.11$). However, despite being small compared to excitatory responses, inhibitory response gains were still significantly greater than without MVP modulation, and response latencies were correspondingly shorter ($p < 0.01$; $F = 7.85$, $F_{crit} = 4.11$). As was true for normal animals, components about axes other than the head rotation axis were small relatively to the main component, indicating a well-aligned 3D VOR.

Fig. 6 shows that after pooling data for acceleration-step responses separately for rotations exciting and inhibiting the implanted labyrinth for each SCC axis, mean G_A and response latencies for the 4 BVD monkeys tested with modulated MVP input were significantly closer to normal for both excitatory and inhibitory rotations than the VOR without modulated MVP input. 3D VOR responses were significantly larger for head rotations that excite the implanted labyrinth (0.69 ± 0.06, 0.62 ± 0.04 and 0.70 ± 0.07 for horizontal, LARP and RALP axes, respectively) than for inhibitory head rotations (0.20 ± 0.02, 0.23 ± 0.01 and 0.20 ± 0.01; $p < 0.01$ in each case for comparison to opposite sense). As exemplified by monkey M067RhF, the overall mean excitatory response G_A was closer to normal for excitatory rotations, but still significantly different from normal ($p < 0.05$). The corresponding mean response latency was also close to normal (9.8, 9.1 and 9.2 ms). Inhibitory response gains were significantly smaller than excitatory ($p < 0.01$ for each stimulus axis), but they were still significantly greater than observed without MVP stimulation ($p < 0.01$ for G_A of each axis), and response latencies trended toward being shorter. (Imprecision of latency measurement for data obtained in BVD animals without MVP input confounds statistical analysis of this difference in latency). As was true for normal animals, components about axes other than the head rotation axis were small relatively to the main component, indicating a well-aligned 3D VOR.

3.3.3. Responses to MVP stimulation are greater when sensory inputs are congruent

While VOR responses of BVD monkeys to sinusoidally modulated MVP input were always greater than for whole-body rotation stimuli presented alone, responses to MVP stimulation depended on whether the MVP stimulus represented a *prosthesis-only* condition (i.e., a modulated MVP stimulus presented to an animal that was in fact stationary) or the typical *combined* condition (i.e., the MVP's modulation encoding head rotation during a real whole-

body rotation stimulus). Fig. 7 shows mean 3D VOR eye responses of monkey M20124RhB after it was rendered BVD via bilateral gentamicin treatment. During 50°/s peak, 2 Hz, passive whole-body rotation in darkness in the *mechanical-only* condition (for which MVP pulse rates were held constant despite the motion), VOR responses were very small (Fig. 7A). During the *prosthesis-only* condition with the MVP delivering pulse rate modulation as though the (truly stationary) animal were undergoing a 50°/s peak, 2 Hz horizontal rotation, a modest and asymmetric response is apparent (Fig. 7B). However, *combined* stimulation elicited a much more robust response (Fig. 7C) than elicited by exactly the same mechanical and MVP stimuli when either was delivered alone.

4. Discussion

These data demonstrate that an MVP can partially restore the 3D VOR for head movements about each SCC axis in rhesus monkeys, albeit with imperfect alignment versus the 3D head rotation axis and with excitation-inhibition asymmetry (e.g., difference in response magnitude for head rotations toward and away from the implanted labyrinth) that becomes prominent during high-acceleration head rotations.

The normal rhesus monkey 3D VOR is quite close to ideal over 0.05–5 Hz and during passive, whole-body acceleration steps of 1000°/s^2 about the horizontal, LARP and RALP SCC axes. While no published 3D data for rhesus monkey responses to LARP and RALP axis rotation are available for comparison, our findings are consistent with rhesus data previously published by other studying rhesus responses to yaw, pitch and roll head rotations (Angelaki and Hess, 1994; Fetter and Zee, 1988; Sadeghi et al., 2006).

Examining the prosthetically-evoked VOR in monkeys undergoing passive whole-body rotation in darkness, we found that gains were about half of normal across 0.05–5 Hz, with an acceleration-dependent asymmetry that became most evident during high-acceleration transient rotations. This is similar to observations in animals with a single normal labyrinth after contralateral labyrinthectomy (Sadeghi et al., 2007) and in humans after unilateral labyrinthectomy (Della Santina et al., 2002) or unilateral treatment with intratympanic gentamicin (Carey et al., 2002). However, asymmetry was typically greater in the prosthetic case than in our unilaterally gentamicin-treated monkeys, probably because (1) rhesus monkeys appeared to suffer only modest degradation of VOR responses after unilateral gentamicin treatment, and (2) withdrawal of MVP excitation to encode inhibitory head rotations probably cannot down-modulate afferent firing rates below a floor of spontaneous natural activity, whereas a single normal labyrinth can (e.g., via down-modulation of hair cell neurotransmitter release). For a unilateral vestibular prosthesis to encode head movements equally well in all directions (including those that normally inhibit canals of the implanted labyrinth), one can set the MVP baseline rate well above the typical resting rate of vestibular nerve afferents, to expand the dynamic range for encoding inhibitory head rotations (e.g., Lewis et al., 2010). However, this strategy often results in greater loss of excitatory responses than improvement in inhibitory responses (Davidovics et al., 2011). Alternate strategies may enhance the ability to encode inhibitory head rotations (e.g., Fridman et al., 2010; Davidovics et al., 2011), but for now the asymmetry of responses to a unilaterally-implanted MVP remains a challenge.

Strikingly better VOR performance during combined body movement and MVP stimulation versus presenting either stimulus alone suggests that the central nervous system integrates input from multiple senses (including residual natural labyrinth activity, electrically-evoked activity, proprioception, and somatosensory input) in a nonlinear way, and that the most robust perception of head movement arises when all inputs are congruent. One candidate site for this integration is the position-vestibular-pause neuron population within vestibular nuclei, which apparently receives labyrinthine, neck proprioceptive and efference copy signals (Sadeghi et al., 2010, 2011a,b). Another candidate could be vestibular nucleus floccular-target neurons, which likely also integrate a range of multimodel sensory input, although their patterns of multisensory integration have not yet been fully described.

Due to their relatively greater availability, we have typically developed, studied and refined MVP paradigms in chinchillas before adapting them to rhesus monkeys. Although the present study was not designed or intended to be a rigorous interspecies comparison, we did note some interesting differences between responses of rhesus monkeys and chinchillas, which differ from rhesus and humans in having a lateral-eyed orientation, little or no stereoscopic vision, and a smaller labyrinth with correspondingly less separation between vestibular nerve branches (Migliaccio et al., 2010). For example, when we applied prosthetic stimulation sufficient to drive a horizontal VOR response gain of 0.4–0.6 at 1 Hz and 50°/s peak in either species, VOR misalignment ranged over 33–42° in chinchillas ($N = 5$, Dai et al., 2011). In contrast, misalignment in rhesus ranged over 21–25° ($N = 4$). Subject to the caveats that electrode array geometry, electrode placement, and current amplitudes could not be made identical in the two species, these results suggest that the MVP-evoked 3D VOR

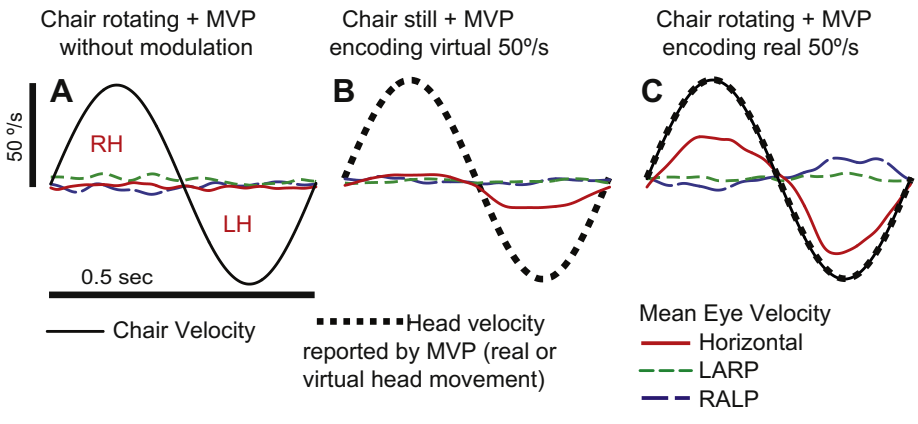

Fig. 7. Mean 3D VOR eye responses of a bilaterally gentamicin-treated rhesus monkey during actual or simulated 50°/s peak, 2 Hz, passive whole-body rotations in darkness. (A) Whole-body rotation only, with MVP set to baseline stimulation. (B) Body stationary but MVP horizontal channel stimulus set to pulse-frequency modulation with the same timing that would usually occur during an actual head rotation of 50°/s peak, 2 Hz. (C) Responses to whole-body rotation with concurrent MVP stimulus rate modulation. The 3D VOR response is much more robust during the combined stimulation and is greater than the sum of responses to either mechanical or electrical stimuli alone.

is better aligned in rhesus monkeys than in chinchillas. Considering that the primate species studied so far normally have *greater* 3D VOR misalignment than do chinchillas (Migliaccio et al., 2010), better alignment of the MVP-evoked 3D VOR in rhesus monkeys compared to chinchillas would probably be due to differences in ampullary nerve stimulation selectivity rather than primate-specific differences elsewhere along the VOR neural pathways. The rhesus labyrinth is about ~1.5–1.7× larger than the chinchilla labyrinth, so a greater separation between target and non-target vestibular nerve branches could make the rhesus labyrinth an easier venue for achieving selective MVP stimulation. If that interpretation is correct, then alignment should be even better in humans, who have ampulla dimensions significantly larger than both chinchillas and rhesus monkeys (Blanks et al., 1985; Ramprashad et al., 1984; Della Santina et al., 2005; Hullar and Williams, 2006).

Acknowledgments

We thank Lani Swarthout for assistance with animal care. This research was supported by the United States National Institutes of Health/National Institute on Deafness and Other Communication Disorders (NIH/NIDCD) grants R01DC0255, R01DC2390, K08DC6216, and 5F32DC009917. Disclosures: inventor status on university-assigned patents related to MVP technology (GYF, BC, CCDS); equity interest in Labyrinth Devices LLC (CCDS).

References

Angelaki, D.E., Hess, B.J., 1994. Inertial representation of angular motion in the vestibular system of rhesus monkeys. I. Vestibuloocular reflex. J. Neurophysiol. 71 (3), 1222–1249.

Blanks, R.H., Curthoys, I.S., Bennett, M.L., Markham, C.H., 1985. Planar relationships of the semicircular canals in rhesus and squirrel monkeys. Brain Res. 340 (2), 315–324.

Carey, J.P., Della Santina, C.C., 2005. Principles of applied vestibular physiology (Chapter 139). In: Cummings, C.W. (Ed.), Cummings Otolaryngology–Head & Neck Surgery, fourth ed. Mosby, Philadelphia, pp. 3115–3159.

Carey, J.P., Minor, L.B., Peng, G.C., Della Santina, C.C., Cremer, P.D., Haslwanter, T., 2002. Changes in the three-dimensional angular vestibulo-ocular reflex following intratympanic gentamicin for Ménière's disease. J. Assoc. Res. Otolaryngol. 3 (4), 430–443.

Chiang, B., Fridman, G., Dai, C., Rahman, M., Della Santina, C.C., 2011. Design and performance of a multichannel vestibular prosthesis that restores semicircular canal sensation in rhesus monkey. IEEE Trans. Neural Syst. Rehabil. Eng., doi:10.1109/TNSRE.2011.2164937.

Dai, C., Fridman, G.Y., Della Santina, C.C., 2010 Dec 31. Effects of vestibular prosthesis electrode implantation and stimulation on hearing in rhesus monkeys. Hear. Res. [Epub ahead of print] PubMed PMID: 21195755; PubMed Central PMCID: PMC3081362.

Dai, C., Fridman, G.Y., Chiang, B., Davidovics, N.S., Melvin, T.A., Cullen, K.E., Della Santina, C.C., 2011. Cross-axis adaptation improves 3D vestibulo-ocular reflex alignment during chronic stimulation via a head-mounted multichannel vestibular prosthesis. Exp. Brain Res. 210 (3–4), 595–606.

Davidovics, N.S., Fridman, G.Y., Chiang, B., Della Santina, C.C., 2011. Effects of biphasic current pulse frequency, amplitude, duration, and interphase gap on eye movement responses to prosthetic electrical stimulation of the vestibular nerve. IEEE Trans. Neural Syst. Rehabil. Eng 19 (1), 84–94.

Della Santina, C.C., Cremer, P.D., Carey, J.P., Minor, L.B., 2002 Sep. Comparison of head thrust test with head autorotation test reveals that the vestibulo-ocular reflex is enhanced during voluntary head movements. Arch. Otolaryngol. Head Neck Surg. 128 (9), 1044–1054. PubMed PMID: 12220209.

Della Santina, C.C., Migliaccio, A.A., Patel, A.H., 2005. Electrical stimulation to restore vestibular function development of a 3-D vestibular prosthesis. Conf. Proc. IEEE Eng. Med. Biol. Soc. 7, 7380–7385.

Della Santina, C.C., Migliaccio, A.A., Patel, A.H., 2007. A multichannel semicircular canal neural prosthesis using electrical stimulation to restore 3-D vestibular sensation. IEEE Trans. Biomed. Eng. 54, 1016–1030.

Fetter, M., Zee, D.S., 1988. Recovery from unilateral labyrinthectomy in rhesus monkey. J. Neurophysiol. 59 (2), 370–393.

Fridman, G.Y., Davidovics, N.S., Dai, C., Migliaccio, A.A., Della Santina, C.C., 2010. Vestibulo-Ocular reflex responses to a multichannel vestibular prosthesis incorporating a 3D coordinate transformation for correction of misalignment. J. Assoc. Res. Otolaryngol. 11 (3), 367–381.

Gillespie, M.B., Minor, L.B., 1999. Prognosis in bilateral vestibular hypofunction. Laryngoscope 109, 35–41.

Grunbauer, W.M., Dieterich, M., Brandt, T., 1998. Bilateral vestibular failure impairs visual motion perception even with the head still. Neuroreport 9 (8), 1807–1810.

Halmagyi, G.M., Curthoys, I.S., 1988. A clinical sign of canal paresis. Arch. Neurol. 45 (7), 737–739.

Haslwanter, T., 1995. Mathematics of three-dimensional eye rotations. Vision Res. 35 (12), 1727–1739.

Hepp, K., 1990. On listing's law. Commun. Math. Phys. 132, 285–295.

Hirvonen, T.P., Minor, L.B., Hullar, T.E., Carey, J.P., 2005. Effects of intratympanic gentamicin on vestibular afferents and hair cells in the chinchilla. J. Neurophysiol. 93 (2), 643–655.

Hullar, T.E., Williams, C.D., 2006. Geometry of the semicircular canals of the chinchilla (*Chinchilla laniger*). Hear. Res. 213 (1–2), 17–24.

Lasker, D.M., Hullar, T.E., Minor, L.B., 2000. Horizontal vestibuloocular reflex evoked by high-acceleration rotations in the squirrel monkey. III. Responses after labyrinthectomy. J. Neurophysiol. 83, 2482–2496.

Lewis, R.F., Haburcakova, C., Gong, W., Makary, C., Merfeld, D.M., 2010. Vestibuloocular reflex adaptation investigated with chronic motion-modulated electrical stimulation of semicircular canal afferents. J. Neurophysiol 103 (2), 1066–1079.

Lyford-Pike, S., Vogelheim, C., Chu, E., Della Santina, C.C., Carey, J.P., 2007. Gentamicin is primarily localized in vestibular type I hair cells after intratympanic administration. J. Assoc. Res. Otolaryngol. 8 (4), 497–508.

Migliaccio, A.A., Todd, M.J., 1999. Real-time rotation vectors. Australas. Phys. Eng. Sci. Med. 22, 73–80.

Migliaccio, A.A., Schubert, M.C., Jiradejvong, P., Lasker, D.M., Clendaniel, R.A., Minor, L.B., 2004. The three-dimensional vestibulo-ocular reflex evoked by high-acceleration rotations in the squirrel monkey. Exp. Brain Res. 159, 433–446.

Migliaccio, A.A., Minor, L.B., Della Santina, C.C., 2010. Adaptation of the vestibulo-ocular reflex for forward-eyed foveate vision. J. Physiol. 588 (20), 3855–3867.

Minor, L.B., 1998. Gentamicin-induced bilateral vestibular hypofunction. J. Am. Med. Assoc. 279, 541–544.

Minor, L.B., Lasker, D.M., Backous, D.D., Hullar, T.E., 1999. Horizontal vestibuloocular reflex evoked by high-acceleration rotations in the squirrel monkey. I. Normal responses. J. Neurophysiol. 82, 1254–1270.

Nguyen, K.D., Minor, L.B., Della Santina, C.C., Carey, J.P., 2009. Time course of repeated intratympanic gentamicin for Ménière's disease. Laryngoscope 119 (4), 792–798.

Ramprashad, F., Landolt, J.P., Money, K.E., Laufer, J., 1984. Dimensional analysis and dynamic response characterization of mammalian peripheral vestibular structures. Am. J. Anat. 169 (3), 295–313.

Remmel, R.S., 1984. An inexpensive eye movement monitor using the scleral search coil technique. IEEE Trans. Biomed. Eng. 31 (4), 388–390.

Robinson, D.A., 1963. A method of measuring eye movement using a scleral search coil in a magnetic field. IEEE Trans. Biomed. Eng. 10, 137–145.

Sadeghi, S.G., Minor, L.B., Cullen, K.E., 2006. Dynamics of the horizontal vestibuloocular reflex after unilateral labyrinthectomy: response to high frequency, high acceleration, and high velocity rotations. Exp. Brain Res. 175 (3), 471–484.

Sadeghi, S.G., Minor, L.B., Cullen, K.E., 2007. Response of vestibular-nerve afferents to active and passive rotations under normal conditions and after unilateral labyrinthectomy. J. Neurophysiol. 97 (2), 1503–1514.

Sadeghi, S., Minor, L.B., Cullen, K.E., 2010. Neural correlates of motor learning: dynamic regulation of multimodal integration in the macaque vestibular system. J. Neurosci 30 (30), 10158–10168.

Sadeghi, S.G., Minor, L.B., Cullen, K.E., 2011a. Multimodal integration after unilateral labyrinthine lesion: single vestibular nuclei neuron responses and implications for postural compensation. J. Neurophysiol. 105 (2), 661–673.

Sadeghi, S.G., Minor, L.B., Cullen, K.E., 2011b. Neural correlates of motor learning in the vestibulo-ocular reflex: dynamic regulation of multimodal integration in the macaque vestibular system. J. Neurosci. 30 (30), 10158–10168.

Straumann, D., Zee, D.S., Solomon, D., Lasker, A.G., Roberts, D.C., 1995. Transient torsion during and after saccades. Vision Res. 35, 3321–3334.

Tweed, D., Cadera, W., Vilis, T., 1990. Computing three-dimensional eye position quaternions and eye velocity from search coil signals. Vision Res. 30 (1), 97–110.